

Asymmetric weak-pinning superconducting channels: vortex ratchets

K. Yu,¹ T. W. Heitmann,¹ C. Song,¹ M. P. DeFeo,¹ B. L. T. Plourde,^{1,*} M. B. S. Hesselberth,² and P. H. Kes²

¹*Department of Physics, Syracuse University, Syracuse, New York 13244-1130, USA*

²*Kamerlingh Onnes Laboratorium, Leiden University,
P.O. Box 9504, 2300 RA Leiden, The Netherlands*

(Dated: October 29, 2021)

The controlled motion of objects through narrow channels is important in many fields. We have fabricated asymmetric weak-pinning channels in a superconducting thin-film strip for controlling the dynamics of vortices. The lack of pinning allows the vortices to move through the channels with the dominant interaction determined by the shape of the channel walls. We present measurements of vortex dynamics in the channels and compare these with similar measurements on a set of uniform-width channels. While the uniform-width channels exhibit a symmetric response for both directions through the channel, the vortex motion through the asymmetric channels is quite different, with substantial asymmetries in both the static depinning and dynamic flux flow. This vortex ratchet effect has a rich dependence on magnetic field and driving force amplitude.

PACS numbers: 74.25.Qt, 74.25.Sv, 74.25.Op

Recently there has been much interest in developing artificial ratchets for generating directed motion using tailored asymmetries [1]. Such ratchets could be used as pathways for producing net transport of matter at the nanoscale. In addition, artificial ratchets can serve as model systems for understanding similar ratchet phenomena in biological systems while allowing for experimental control over many of the ratchet parameters [2]. A variety of ratchets have been considered, but one particular type that has been implemented in several different systems is the rocking ratchet, where a spatial asymmetry is engineered into the potential energy landscape governing particle motion and an external control variable can be adjusted to tilt this potential. The application of an oscillatory drive of the control variable with zero mean can result in the net motion of particles through the potential because of the different rates for overcoming the barriers in the two directions through the ratchet.

Implementations of ratchets in solid-state devices include asymmetric structures of electrostatic gates above a two-dimensional electron gas [3], and arrays of Josephson junctions with asymmetric critical currents [4]. Structures have also been developed for producing a ratchet effect with vortices in superconducting thin films involving either asymmetric arrangements of pinning centers [5, 6] or asymmetric magnetic pinning structures [7]. In this Communication, we describe a vortex ratchet using two-dimensional guides to generate asymmetric channels for vortex motion. In our structures, the potential asymmetries arise from differences in the interaction strength between vortices and the channel walls, resulting in a substantial ratchet effect for the motion of vortices through the channels. Our design is related to a previous vortex ratchet proposal [8], although our ratchet is in a somewhat different parameter regime.

Nanoscale channels for guiding vortices through superconducting films with a minimal influence from pin-

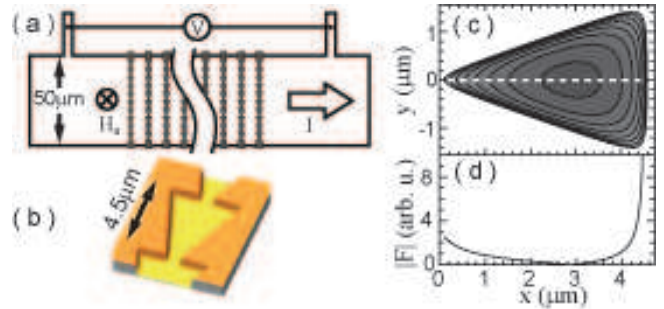


FIG. 1: (Color online) (a) Schematic of strip with ratchet channels; channel spacing is $10 \mu\text{m}$. (b) AFM image of one ratchet cell; channel depth is 88 nm . (c) Contour plot of model potential for vortex interacting with ratchet cell walls. (d) Magnitude of corresponding force along center of channel.

ning have been developed for studies of vortex matter in confined geometries, including experiments on melting [9], commensurability [10], and mode locking [11]. Such channels are fabricated from bilayer films of amorphous-NbGe, an extremely weak-pinning superconductor, and NbN, with relatively strong pinning. A reactive ion etching process removes NbN from regions as narrow as 100 nm , defined with electron-beam lithography, to produce weak-pinning channels for vortices to move through easily. In contrast, vortices trapped in the NbN banks outside of the channels remain strongly pinned.

We have fabricated weak-pinning channels with 200 nm -thick films of a-NbGe and 50 nm -thick films of NbN on a Si substrate, and we have designed many of the channels such that the walls have an asymmetric sawtooth pattern (Fig. 1). Our layout consists of a strip with multiple pairs of probes for sensing the voltage drop V due to vortex motion. A transport current driven through the strip with an external supply generates a transverse Lorentz force on the vortices. Between each

pair of voltage probes is an array of identical channels – one array consists of 50 channels each with a constant width of $2\ \mu\text{m}$; another array has 30 ratchet channels with the dimensions described in Figure 1; yet another array contains 30 identical ratchet channels, all oriented in the opposite direction across the strip. We perform our measurements with the strip immersed in a pumped helium bath with a temperature stability of $0.2\ \text{mK/hr}$. Our results presented here were obtained at $T = 2.78\ \text{K}$, and our measured transition temperature for the a-NbGe is $T_c = 2.88\ \text{K}$. For each measurement sequence, the strip was heated to $\sim 15\ \text{K}$, above T_c of both the NbGe and NbN films, and was then cooled in zero applied magnetic field; a μ -metal shield reduced the background magnetic field below $13\ \text{mG}$. All field-dependence data were acquired while increasing the magnetic field H_a from zero, where we generate H_a with a superconducting coil.

One can expect such asymmetric channel structures to influence vortex dynamics if the confinement from the channel walls distorts the screening currents that circulate around each vortex differently depending on the motion of the vortex through the channel. At the temperature of our measurements, we estimate the penetration depth of the NbN to be $\lambda_{\text{NbN}} \approx 0.5\ \mu\text{m}$ and that of NbGe to be $\lambda_{\text{NbGe}} \approx 1.9\ \mu\text{m}$, based on the film parameters and the standard dirty-limit expressions and assuming a two-fluid model for the temperature dependence. Furthermore, the thin-film penetration length, $2\lambda^2/d$, that sets the characteristic extent for the screening currents around a vortex in a thin film is $\sim 42\ \mu\text{m}$ for the NbGe in the channels, clearly much greater than the width of the channels, such that the shape of the channel walls will play an important role in distorting each vortex. The interaction of a vortex with the channel walls can be understood by considering the model of Mkrtchyan *et al.* for the interaction between a vortex and the interface between two superconductors with different penetration depths [12]. For our strips, the channel corresponds to the superconductor with the larger penetration depth, while the NbN banks have the shorter penetration depth. According to the Mkrtchyan model, a vortex in the channel will experience a repulsive interaction U_i from the i^{th} wall a distance d_i away keeping the vortex in the channel,

$$U_i \propto \left(\frac{\lambda_{\text{NbGe}}^2 - \lambda_{\text{NbN}}^2}{\lambda_{\text{NbGe}}^2 + \lambda_{\text{NbN}}^2} \right) \ln \left(\frac{\lambda_{\text{NbGe}}}{d_i} \right). \quad (1)$$

If we consider a single vortex located in one of the ratchet cells, we can make a crude model of the potential energy landscape by summing the contributions from the interaction of the vortex with each of the three walls of the ratchet cell, ΣU_i [Fig. 1(c)]. The derivative of this potential along the central symmetry line of the cell exhibits an asymmetric force on the vortices [Fig. 1(d)]. Thus, the two sloped walls result in a gradual increase in the potential energy as the vortex approaches the aperture in the “easy” direction, while the potential energy

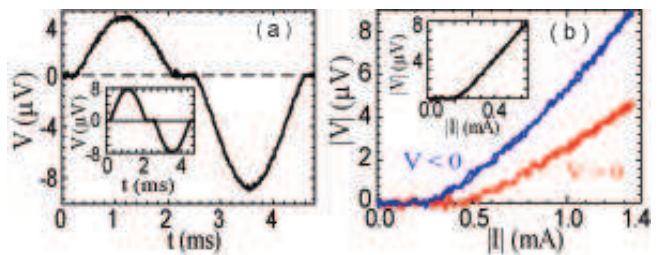


FIG. 2: (Color online) (a) $V(t)$ for ratchet channels with sinusoidal current drive $I(t)$; $I_{ac} = 1.35\ \text{mA}$. (Inset) $V(t)$ for $2\ \mu\text{m}$ -wide uniform channels; $I_{ac} = 0.59\ \text{mA}$. (b) IVC for ratchet plotted with positive and negative branches in first quadrant for comparison. (Inset) corresponding IVC for $2\ \mu\text{m}$ -wide uniform channels, also with both branches in first quadrant. $H_a = 4.20\ \text{Oe}$ in all plots.

grows abruptly as the vortex approaches the wide back wall of the ratchet cell for motion in the “hard” direction.

The vortex dynamics in the channels can be characterized by measuring V , which is proportional to the vortex velocity and density. We measure V with a room-temperature amplifier and we drive the vortices by applying 200 cycles of a bias current sine wave $I(t)$ at $210\ \text{Hz}$ with amplitude I_{ac} . We average the resulting voltage response to obtain a $V(t)$ curve for one period. For the uniform channels, this is always symmetric about $V = 0$, while for the ratchets, one side of the curve typically has a larger response than the other [Fig. 2(a)]. We combine this resulting $V(t)$ curve with $I(t)$ to obtain a current-voltage characteristic, IVC. By plotting the negative and positive branches of the IVC both in the first quadrant, the substantial asymmetry of the response for the ratchet channels is apparent, while the corresponding IVC for the uniform-width channels is symmetric [Fig. 2(b)]. Furthermore, from the IVC for the ratchet channels, there are clear asymmetries both in the critical currents at which the vortices begin to depin from the static state and in the flux flow resistances, inversely related to the vortex dynamic friction in the channels.

We characterize the transition from the static state to a dynamical flux flow regime by measuring the critical current in the conventional way, that is, by measuring the IVC as described earlier, then using a $1\ \mu\text{V}$ criterion to define the critical current I_c . Measurements of the field dependence $I_c(H_a)$ on the $2\ \mu\text{m}$ -wide uniform channels display a similar response to that characteristic of an edge barrier for a thin, weak-pinning superconducting strip in a perpendicular magnetic field, where the entry of vortices at the strip edge is determined by the distortion of the current density across the width of the strip [13, 14]. I_c is a maximum at $H_a = 0$, where I_c is due to the entry of vortices and antivortices at opposite edges of the strip due to the self-field of I . As H_a is increased, $I_c(H_a)$ initially decreases linearly, as the self-field and H_a add with the same sense at one edge and are able to ex-

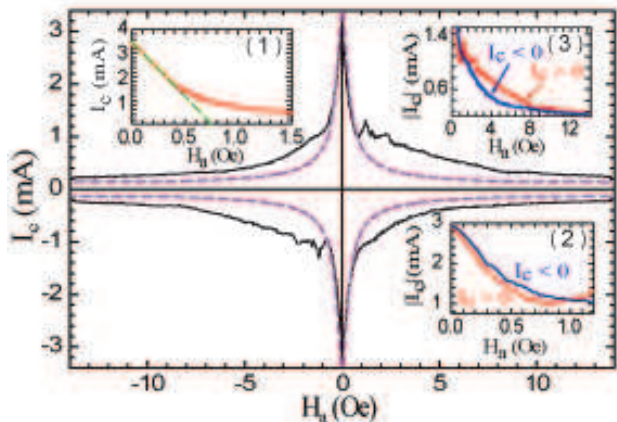


FIG. 3: (Color online) Critical current variation with H_a – ratchet channels (black) and uniform-width channels (magenta, dashed). (Inset 1) $I_c(H_a)$ for uniform-width channels at low magnetic fields along with linear fit. Ratchet $I_c(H_a)$ for both senses of I at (Inset 2) small H_a , (Inset 3) large H_a .

ceed the vortex entry condition for progressively smaller I . In this regime, there are no vortices present in the strip for $I < I_c$, while larger currents result in a dynamical flux flow state with vortices entering the strip at one edge and moving across to the other edge. For larger H_a , the external field can be sufficient to push vortices into the strip, even for $I = 0$, and these vortices arrange in a static dome-shaped structure in the middle of the strip [14, 15]. When $I \neq 0$, the dome shifts towards one edge and I_c is reached when the self-field plus H_a at the opposite edge overcome the entry barrier to allow new vortices to enter. In this regime, I_c decreases like H_a^{-1} [13]. The measurements of $I_c(H_a)$ for the $2 \mu\text{m}$ -wide uniform channels follow essentially this behavior and I_c is symmetric with the direction of I and the sense of H_a (Fig. 3), indicating that the channels are symmetric and the strip edges at the ends of the channels do not have any significant roughness asymmetries. This is consistent with the entry of vortices only into the channels at the edge of the strip, and not into the strong-pinning NbN banks, as one would expect at the relatively small magnetic fields of our experiment, based on the lower edge barriers at the channel edges compared to the thicker NbN banks.

For the ratchet channels, I_c is also a maximum at $H_a = 0$, with an initial linear decrease as H_a is increased, however, in contrast to the uniform-width channels, I_c is weakly asymmetric with a $\sim 15\%$ difference for the two polarities of I . In this low-field regime, where I_c corresponds to the entry of vortices into the vortex-free state of the channels, the smaller I_c has the sense of the bias current pushing the vortices in the hard direction of the ratchet. When H_a is reversed, the sense with the smaller I_c inverts as well, again corresponding to vortex motion

in the hard direction. For larger magnetic fields, $I_c(H_a)$ deviates from a linear decrease, as in the uniform-width channel measurements when a static vortex dome can be formed in the channels before I reaches I_c . However, in this regime the ratchet channel I_c develops a substantial asymmetry with respect to the sense of I . Now I_c for the sense of I pushing vortices in the hard direction becomes considerably larger than that for the easy direction and exhibits a sequence of peaks. Thus, at the start of this regime, the critical currents for the two directions of vortex motion actually cross [Fig. 3(inset 2)]. In this regime, vortices sit statically in the ratchet channels for $I < I_c$, and thus can explore the asymmetry due to the shape of the ratchet channel walls as I is increased [Fig. 1], such that vortices dip and flow at a smaller I when the Lorentz force is oriented in the easy direction. This is consistent with the antisymmetry of $I_c(H_a)$, that is, for the opposite sense of H_a , the smaller I_c occurs for the opposite sense of I , and thus the same spatial direction through the ratchet. We observe an identical response, but with the opposite sign for ratchet channels with the same geometry but the opposite direction of ratchet cells at a different location on the same strip (not shown).

The abrupt crossing of I_c for the two senses of current corresponds to the first entry of a vortex into each ratchet channel for $I < I_c$ and the peak structure in I_c for the hard direction of the ratchet is likely due to the entry of subsequent vortices into each ratchet channel. For small H_a , below this crossover of the two senses of I_c , where no vortices are present in the channels for $I < I_c$, there are screening currents flowing along the channel walls due to the discontinuity in thickness and penetration depth at each wall. These currents will be concentrated at the outer points of each ratchet cell and can effectively invert the sense of the ratchet potential defined by the shape of the channel walls, thus reversing the ratchet effect for the vortices that enter the channels when $I > I_c$. For larger H_a , the interaction of the circulating currents for each vortex in the channel with the walls dominates and the ratchet effect exhibits the sign expected from the spatial asymmetry of the channel pattern.

In addition to the asymmetric response of $I_c(H_a)$ for the ratchet channels, we also observe substantial asymmetries in the dynamical flux-flow state. A general method to characterize asymmetries in both static and dynamic properties involves averaging $V(t)$ over a complete cycle, such as the trace in Fig. 2(a), to obtain V_{dc} . For a value of H_a corresponding to the IVC of Figure 2 for the ratchet channels, V_{dc} will clearly be non-zero, while for uniform-width channels, we always observe $V_{dc} = 0$ for all H_a . We map the variation of V_{dc} with H_a and I_{ac} for the ratchet channels (Fig. 4) by zero-field cooling, then measuring $V_{dc}(I_{ac})$ while incrementing H_a towards positive values. We zero-field cool again to measure the $H_a < 0$ response by incrementing H_a from zero towards negative values. For each H_a , we perform our standard

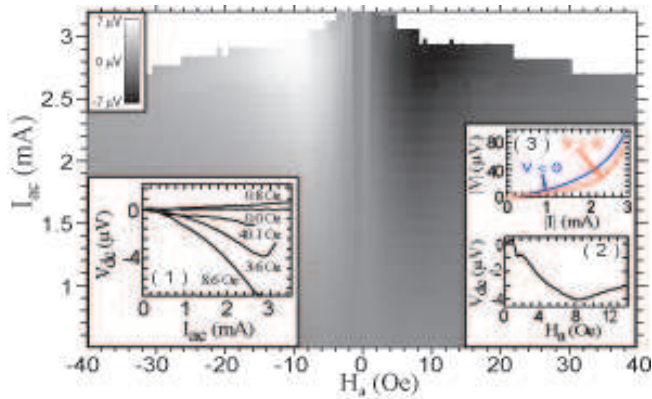


FIG. 4: Density plot of V_{dc} vs. I_{ac} and H_a . (Inset 1) Line cuts of $V_{dc}(I_{ac})$ for indicated values of H_a . (Inset 2) $V_{dc}(H_a)$ line cut at $I_{ac} = 2.1$ mA. (Inset 3) IVC for $H_a = 8.6$ Oe at measured for large I_{ac} .

measurement of V_{dc} using a burst of sinusoids with amplitude I_{ac} while stepping to progressively larger values of I_{ac} . We continue to increase I_{ac} , thus increasing the vortex velocity through the channels, until an instability occurs and the channels switch out to the normal conducting state. The switching point is independent of the frequency of our $I(t)$ sinusoid, at least up to 30 kHz, and the sample is immersed in liquid helium, thus making simple Joule heating unlikely as the cause. Instead, the curvature in the IVC at large I_{ac} [Fig. 4(inset 3)] suggests that the switching is related to the Larkin-Ovchinnikov vortex core instability mechanism [16], perhaps with a related self-heating effect as evidenced by the H_a -dependence of the maximum I_{ac} visible in Figure 4 [17].

For any H_a , $V_{dc}(I_{ac})$ is generally zero for small I_{ac} , when $I < I_c(H_a)$ for both polarities. For larger I_{ac} , $|V_{dc}|$ tends to grow, and for certain H_a , $|V_{dc}|$ eventually begins to decrease before the channels switch out to the normal state [Fig. 4(inset 1)]. In general, V_{dc} is antisymmetric with H_a , thus indicating that the direction for net vortex motion corresponds to the same spatial direction through the ratchet channels. There are also substantial peaks in $|V_{dc}|$ visible on either side of $H_a = 0$, thus there is an H_a that optimizes the ratchet effect (Fig. 4). For $H_a = 0$, $V_{dc} \approx 0$ for all I_{ac} , as there are no screening currents flowing along the channel walls in response to H_a . For $H_a \neq 0$ but small, the sign of V_{dc} corresponds to the net motion of vortices in the hard direction, consistent with the reversal of the critical currents observed in the measurements of $I_c(H_a)$ [Fig. 3(inset 2)]. There is an abrupt transition of V_{dc} to the expected sign for net vortex motion in the easy direction at $H_a \approx \pm 1$ Oe and this can be seen as vertical ridges in Figure 4.

By comparing line cuts of $V_{dc}(H_a)$ for a particular value of I_{ac} [Fig. 4(inset 2)] with the measurements of $I_c(H_a)$ [Fig. 3(inset 3)], we observe that the value of H_a at which $|V_{dc}|$ reaches the maximum ($H_a = 8.6$ Oe)

coincides with the approximate convergence of the two senses of I_c . A rough extrapolation from the peak structure in $I_c(H_a)$ indicates that the maximum in $|V_{dc}|$ occurs approximately at the matching point of one vortex per ratchet cell. Thus, at this point, the arrangement of vortices minimizes the asymmetry in the static friction, as characterized by I_c , yet the overall ratchet response, as captured by $|V_{dc}|$ is a maximum, due to the substantial asymmetry in this regime between the dynamical sliding states for the two directions. The two branches of the IVC measured with a large I_{ac} [Fig. 4(inset 3)] exhibit a considerable difference in curvature and this dynamical asymmetry results in the significant ratchet response.

In summary, we have demonstrated a substantial ratchet effect for a system of vortices moving through weak-pinning channels with asymmetric walls. This ratchet exhibits considerable asymmetries in both the static and dynamic friction, with different dependences on H_a . The edge barrier corresponding to the strip geometry of our structure has an important role in the vortex dynamics, including delineating a low-field Meissner regime in the channels from a state corresponding to vortices occupying ratchet cells statically for $I < I_c$. However, asymmetries in the edge barriers alone, as described by the model of Ref. [18], cannot account for our ratchet effect, although this may be related to the smaller reverse ratchet response that we observe at small H_a in the Meissner regime of the channels. The microfabricated nature of our channels allows for future ratchet explorations with different channel wall shapes and configurations.

This work was supported by the National Science Foundation under Grant DMR-0547147. We acknowledge use of the Cornell NanoScale Facility.

* bplourde@phy.syr.edu

- [1] P. Hänggi, F. Marchesoni, and F. Nori, *Ann. Physik* **14**, 51 (2005).
- [2] R. D. Astumian, *Science* **276**, 917 (1997).
- [3] H. Linke, T. E. Humphrey, A. Löfgren, A. O. Sushkov, R. Newbury, R. P. Taylor, and P. Omling, *Science* **286**, 2314 (1999).
- [4] D. E. Shalóm and H. Pastoriza, *Phys. Rev. Lett.* **94**, 177001 (2005).
- [5] J. V. de Vondel, C. C. de Souza Silva, B. Y. Zhu, M. Morelle, and V. V. Moshchalkov, *Phys. Rev. Lett.* **94**, 057003 (2005).
- [6] Y. Togawa, K. Harada, T. Akashi, H. Kasai, T. Matsuda, F. Nori, A. Maeda, and A. Tonomura, *Phys. Rev. Lett.* **95**, 087002 (2005).
- [7] J. E. Villegas, S. Savel'ev, F. Nori, E. M. Gonzalez, J. V. Anguita, R. Garca, and J. L. Vicent, *Science* **302**, 1188 (2003).
- [8] J. F. Wambaugh, C. Reichhardt, C. J. Olson, F. Marchesoni, and F. Nori, *Phys. Rev. Lett.* **83**, 5106 (1999).
- [9] R. Besseling, N. Kokubo, and P. H. Kes, *Phys. Rev. Lett.* **91**, 177002 (2003).

- [10] A. Pruymboom, P. H. Kes, E. van der Drift, and S. Radelhaar, *Phys. Rev. Lett.* **60**, 1430 (1988).
- [11] N. Kokubo, R. Besseling, V. M. Vinokur, and P. H. Kes, *Phys. Rev. Lett.* **88**, 247004 (2002).
- [12] G. S. Mkrtchyan, F. R. Shakirzyanova, E. A. Shapoval, and V. V. Schmidt, *Zh. Eksp. Teor. Fiz* **63**, 667 (1972).
- [13] B. L. T. Plourde, D. J. Van Harlingen, D. Y. Vodolazov, R. Besseling, M. B. S. Hesselberth, and P. H. Kes, *Phys. Rev. B* **64**, 014503 (2001).
- [14] D. Y. Vodolazov and I. L. Maksimov, *Physica C* **349**, 125 (2000).
- [15] M. Benkraouda and J. R. Clem, *Phys. Rev. B* **58**, 15103 (1998).
- [16] A. I. Larkin and Y. N. Ovchinnikov, *Zh. Eksp. Teor. Fiz.* **68**, 1915 (1975).
- [17] A. Bezuglyj and V. Shklovskij, *Physica C* **202**, 234 (1992).
- [18] D. Y. Vodolazov and F. M. Peeters, *Phys. Rev. B* **72**, 172508 (2005).